Earth and Planetary Science Letters 502 (2018) 104–114

Contents lists available at ScienceDirect

Earth and Planetary Science Letters

www.elsevier.com/locate/epsl

Seismo-acoustic signals of the Baumgarten (Austria) gas explosion detected by the AlpArray seismic network

Felix M. Schneider *,[1], Florian Fuchs *, Petr Kolínský, Enrico Caffagni, Stefano Serafin [2], Manfred Dorninger, Götz Bokelmann, AlpArray Working Group [3]

Department of Meteorology and Geophysics, University of Vienna, Austria

ARTICLE INFO

Article history:
Received 14 May 2018
Received in revised form 30 July 2018
Accepted 21 August 2018
Available online 13 September 2018
Editor: J.-P. Avouac

Keywords:
seismo-acoustic coupling
infrasound
explosion
accident
AlpArray

ABSTRACT

On December 12, 2017 a devastating release and combustion of gas occurred at the Baumgarten gas hub in Eastern Austria, which is a major European distribution node for natural gas. We have detected the resulting seismo-acoustic signal on permanent and temporary broadband seismic stations at distances between 30 and 175 km from the gas hub, most prominently in the 2–4 Hz range. Two distinct phase arrivals correspond to acoustic waves traveling through the troposphere and stratosphere. The passing of a cold front shortly before the explosion led to several temperature inversions at low altitude, and acoustic waveguides within the troposphere that facilitated our infrasound detections at distances as close as 50 km from the source, in addition to the commonly observed stratospheric reflections. 3D acoustic raytracing using temperature and wind velocities from the HRES (high-resolution) forecast model of the European Center for Medium Range Weather Forecast (ECMWF) has allowed to precisely relate the spatial distribution of our detections with calculated surface bounce points of infrasound rays. This has provided a precise and independent estimate of the time of the accident, to be used in forensic investigations. In addition to the acoustic signal we find evidence for weak seismic phases on the stations closest to the gas hub, yet the sudden release of gas above the surface generated acoustic waves more effectively than seismic waves. After the first explosion signal, we also detect a prolonged coda of elevated noise, which is probably due to ongoing gas release and/or the fire from the escaping gas. Systematic analyses like the one conducted here are of great value to detect, locate, and characterize anthropogenic sources at a regional scale.

1. Introduction

Seismic monitoring has proven very useful not only for detecting earthquakes, but also to observe other types of seismic sources, from different natural causes to human activity. Within that wide range of applications the study of both deliberate and accidental explosions has a particular role, due to the need to investigate such incidents using all available information. Case studies where seismology provided unique insight have included accidental explosions of pipelines (Koper et al., 2003; Evers et al., 2007), of industrial plants (Ceranna et al., 2009; Ottemöller and Evers, 2008), of ammunition depots/factories and of war remnants (Kristekova et al., 2008; Green et al., 2011; Hinzen, 2014) as well as the sinking of submarines or ships (Koper and Wallace, 2001; Hong, 2011), and military and/or terrorist activity (Aleqabi et al., 2015; Koper et al., 1999, 2002).

Seismological measurements are particularly useful, if they are not only available from single seismometers, but from distributed networks, as demonstrated using the USArray (Walker et al., 2011; Nippress et al., 2014; Chunchuzov et al., 2014; Hedlin and Drob, 2014). The recently installed AlpArray network across the European Alps (Hetényi et al., 2018) is so far the largest dense deployment of that kind in Europe. It consists of 628 broadband seismic 3-component stations, and has an average station spacing of around 40 km. The primary purpose of the network is the study of the subsurface under the Alpine region; yet the dense station spacing makes it attractive also for investigating other geophysical phenomena.

* Corresponding authors.
E-mail addresses: felix.m.schneider@gmx.de (F.M. Schneider), florian.fuchs@univie.ac.at (F. Fuchs).
[1] Current address: Helmholtz Centre Potsdam – GFZ German Research Centre for Geosciences, Potsdam, Germany.
[2] Current address: Department of Atmospheric and Cryospheric Sciences, University of Innsbruck, Innsbruck, Austria.
[3] www.alparray.ethz.ch.

https://doi.org/10.1016/j.epsl.2018.08.034

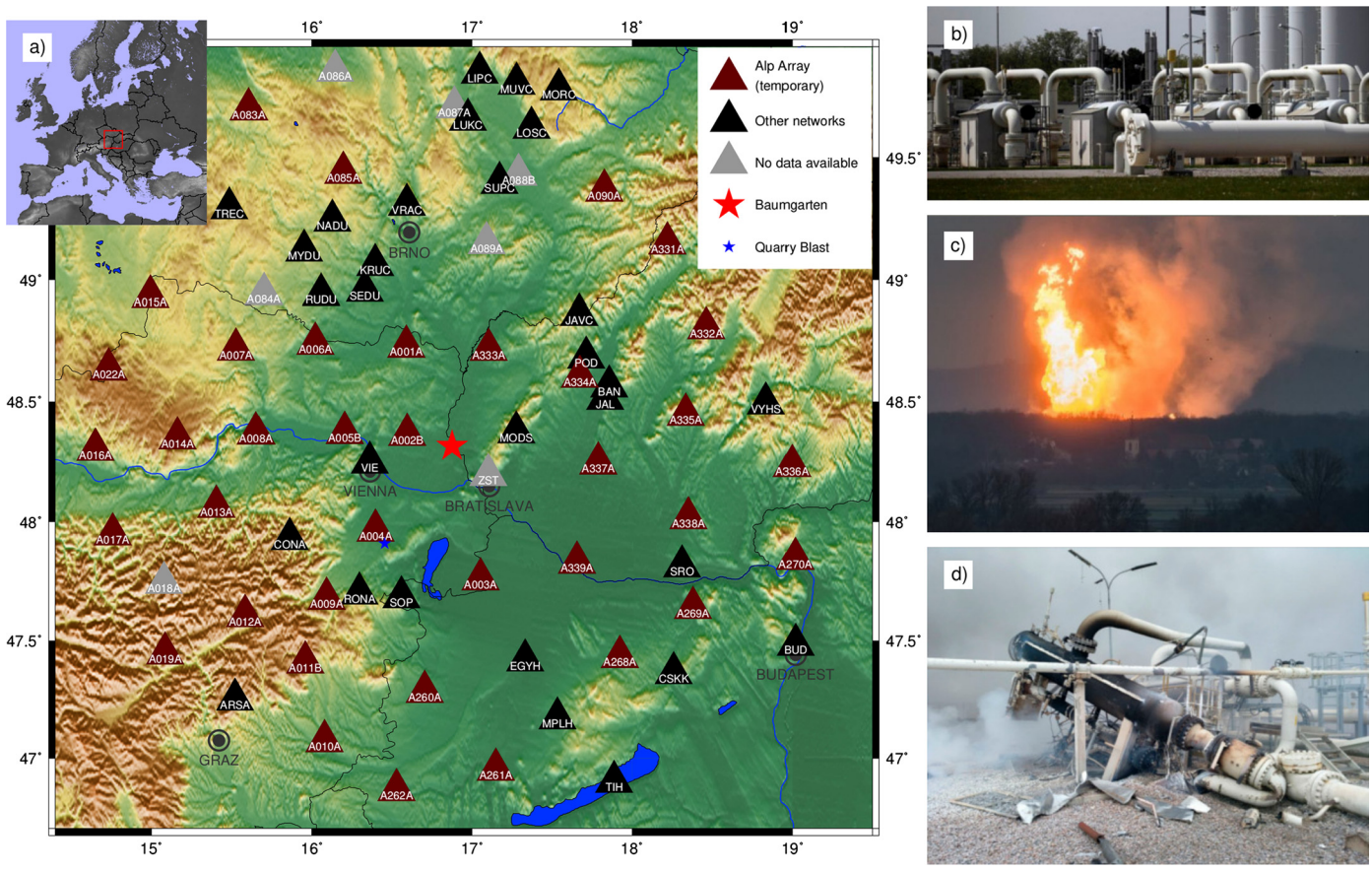

Fig. 1. a) Map of the seismic stations (triangles) in the wider Vienna region used for this study from AlpArray and other networks. The location of the Baumgarten gas explosion is marked by the red star. The inset shows the position of the study area within Europe. All stations are marked with names. Station names following the scheme AxxxA, with xxx being digits only, denote temporary AlpArray stations (network code Z3), while all other stations are associated with various permanent networks (for network codes see Acknowledgments). b) Intact gas filtering devices at the Baumgarten gas hub before the explosion.[5] c) The fire during the explosion as seen from larger distance.[6] d) Destroyed gas filter device after the explosion.[7]

We report here about a study of infrasound and seismic waves from Eastern Austria, which has shown the capability of the AlpArray network to detect seismo-acoustic waves, and to contribute to investigations of human accidents. On December 12, 2017 a devastating release and combustion of gas occurred at the Baumgarten gas hub in Eastern Austria. The Baumgarten gas hub is located 35 kilometers to the North-East of Vienna, near the Austria–Slovakia border (see Fig. 1); it is one of the major distribution hubs for natural gas in Europe. With an annual transported volume of 40 billion cubic meters (equivalent to 10% of Europe's gas demand) it is Austria's main reception point for natural gas imports, especially from Russia and Norway.[2] The majority of the gas is transported to other European countries, in particular Germany, Italy and Hungary.

In this paper, we begin with a ground truth description of the incident; then we focus on the characteristics of the seismic data. We introduce the raypath modeling we performed, and the meteorological data that were used, and compare the observations with the predicted arrivals. We will show how the origin time can be determined best by using the entire timefield of the acoustic waves. A supplementary section shows all analyzed data and briefly discusses additional information, e.g. comparison of the meteorological forecast model with measured balloon data, and more details on the determination of the origin time.

2. Ground truth

On December 12, 2017 around 07:45 UTC (time of the first emergency call) a devastating release and combustion of gas occurred at the Baumgarten gas hub (see Fig. 1). The incident caused one fatality and left over 20 people injured.[3] As news about the incident spread, the price for natural gas temporarily increased by more than 80% on several gas exchange markets in Europe.[4] While commonly termed "The Baumgarten explosion" the incident was technically not an explosion. Rather, according to forensic on-site investigations, highly pressurized gas was released very suddenly and forcefully blown out of a gas filtering device located above ground and was subsequently set on fire. A missing safety bolt at one of the closing lids resulted in failure of the lid at a pressure of few tens of bars, and gas got suddenly released. The lid forcefully crashed into a second filter device located opposite at several meters distance. Highly pressurized gas was released from the second device as well. Likely, the impact of the first metallic lid onto the second created sparks which ignited the gas. However, since

[2] https://www.gasconnect.at/fileadmin/Broschueren-Folder/GCA_2016-04_Baumgarten_EN_web.pdf.

[3] https://www.nytimes.com/2017/12/12/world/europe/austria-gas-explosion.html.

[4] https://www.theguardian.com/world/2017/dec/12/italy-declares-state-emergency-gas-explosion-austria.

[5] http://www.heute.at/welt/news/story/Italien-erklaert-Notstand-nach-Gasexplosion-bei-OMV-49525073.

[6] https://diepresse.com/home/panorama/oesterreich/5336872/Explosion-in-Gasstation-Baumgarten-fordert-ein-Todesopfer.

[7] http://www.noen.at/gaenserndorf/verheerende-explosion-opfer-mehrheitlich-gas-connect-mitarbeiter/70.752.356.

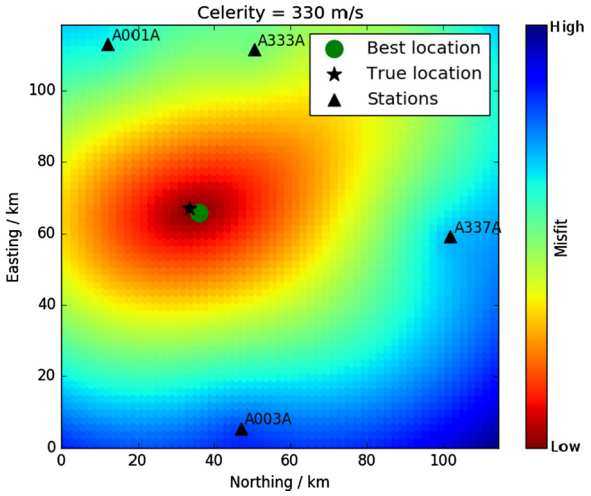

Fig. 2. Result of grid search for source location using first onset picks (with 2 × 2 km grid interval, 2 s time step, acoustic velocity fixed to 330 m/s). The resulting location is 3 km from true location.

the gas was blown out of the filtering tube at very high pressure it could not explosively combust. Only more than hundred meters from the point of release the violent gas stream started burning. Temperatures of up to almost 1000 °C melted plastic parts of cars parked in the vicinity. Eyewitnesses reported a several-meter-high flame burning for 15–20 min, which was visible also from Vienna (at about 35 km distance), before it got extinguished.

3. Detection of seismo-acoustic data

We use seismic waveform data mainly obtained from the AlpArray network, which is operated by 24 European research institutions and seismological services (Hetényi et al., 2018). The seismic network comprises both permanent and temporary installations and covers the entire Alpine orogen including the neighboring forelands with a homogeneous station spacing of less than 40 km. Thus, the AlpArray network encompasses the site of the Baumgarten gas hub on the border between Austria and Slovakia. Additionally, we analyzed waveform data from several local small-scale short-period arrays to increase the spatial sampling wherever possible (see Fig. 1). The majority of waveform data for this study is obtained from three-component broad-band sensors and continuously sampled at 100 Hz sampling rate. Please refer to the Data availability section for more information and details on data access.

We manually inspected the seismic records of 68 stations installed within a 185 km radius of the Baumgarten gas hub and providing data for the day of interest (see Fig. 1 and supplementary Fig. S1). After the first screening for a seismic phase on the closest stations to Baumgarten was not successful, we found an impulsive arrival with high signal to noise ratio on four stations (A001A, A333A, A337A, and A003A) located on a semicircle covering north–northwestern to eastern and southern directions around Baumgarten with distances ranging from 45 to 70 km. In contrast, no such signal could be detected on stations in western directions in the same distance range (A005B, A002B, VIE). We derived the apparent velocity of the signal by comparing the detection times with respect to each other, taking into account the station distances from the known explosion origin at the Baumgarten gas hub. Since the apparent velocities for the detected arrivals were in the range of 350–360 m/s it was evident that the signal is of seismo-acoustic origin. It propagated as infrasound rather than as seismic wave. We manually picked the first onset of the signal for the first four detections and used them to locate the epicenter of the event by grid search, assuming a constant speed of sound of 330 m/s (see Fig. 2). This confirmed the source of the detected signals to be located at the Baumgarten gas hub.

Tracing the apparent velocities of 350–360 m/s on a seismic record section sorted by distance yielded many more candidate detections of the same phase as well as a second later phase at more distant stations, showing a similar apparent velocity. We performed forward modeling of the acoustic waves by raytracing (see Section 4 and Fig. 3) which together with the onset picks from the detected signals provided a first estimate of the origin time. While the apparent velocity is a measure derived by comparing arrival times on different stations, the celerity is defined by the ratio of distance to travel-time, which is measured individually at each station for a given origin time. Based on our preliminary origin time we were able to search more specifically for detections in specific time ranges expected from the celerities of certain infrasound wave guides (time windows marked with green and blue colors in Fig. 4 and supplementary Fig. S1). Depending on the distance of the stations, we eventually detected impulsive signals in the two celerity ranges of 318–346 m/s and 275–310 m/s, which can be attributed to tropospheric and stratospheric guided waves, respectively (Ceranna et al., 2009). Finally, the additional detections contributed to a refined origin time estimate (see Section 5).

Following the scheme described above, we detected two phase arrivals of a characteristic impulsive signal that is very likely associated to the Baumgarten accident on 25 seismic stations in up to 175 km distance from the gas hub (see Figs. 4 and 5). The spatial distribution of the detections is highly asymmetric with the majority of detections in northern and eastern directions from the gas hub and almost no detections to the west of the gas hub. The faster phase is clearly detected on 17 stations (green and violet triangles in Fig. 5) mainly at closer distances (in less than 80 km distance), but in northern and southern directions also at large distances (>100 km). The later phase is clearly observed at 11 stations (blue and violet triangles in Fig. 5) and only at distances larger than 100 km in eastern and south eastern directions. Three stations (violet triangles in Fig. 5) detected both phases. On the majority of stations the explosion signal is most prominent (with best signal-to-noise ratio) within the 2–4 Hz frequency range. Here, the phase identification was done manually. Even so, an automatic procedure taking into account peak-signal to noise ratios could yield a very similar detection/non-detection pattern, see supplementary Fig. S2.

After the main impulsive seismo-acoustic arrival we observed elevated noise levels for approximately 19 min on three stations with good signal-to-noise ratios (see Fig. 6). In the waveforms this continuation of the explosion signal is evident in form of increased background amplitudes. A spectrogram view of the data from station A001A shows that amplitudes over a wide frequency range from approximately 3 Hz to 20 Hz are increased for the duration of this extended coda signal.

For the six stations with positive detections closest to the explosion we checked the polarization of the seismo-acoustic signal for a 0.5 s time window (data bandpass-filtered from 2–4 Hz). Within the first onset as well as within the phase of maximum amplitudes all such signals are radially polarized and align well with the expected direction of propagation from the gas hub (see Fig. 7). Polarization along the vertical-radial plane (Z vs. R) does, however, not show any clear common polarization or particle motion features. Based on the origin time from the acoustic signal we revisited the records of the closer stations for a purely seismic signal originating from the gas explosion. On three close stations in distances ranging from 20 to 50 km from the gas explosion we find, after all, weak seismic arrivals in the 0.6–1 Hz frequency band that are radially polarized along the expected propagation path, show retrograde particle motion and propagate (based on the estimated origin time) with seismic group velocities of approximately

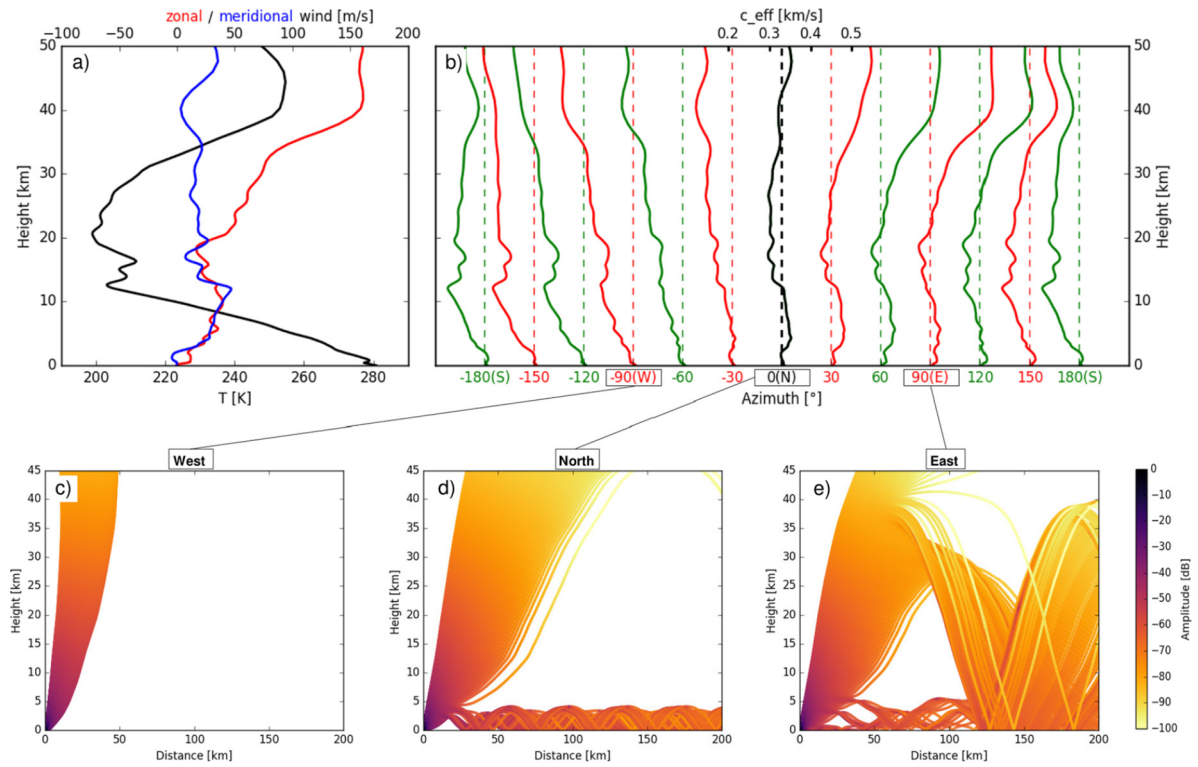

Fig. 3. a) Atmospheric height profiles for temperature, zonal (longitude-parallel) and meridional (latitude-parallel) wind, from ECMWF forecast model for Dec. 12 2017, 8:00 UTC at closest grid-point to the explosion (5 km to the north at lat. 16.875°, long. 48.375°). b) Derived effective sound speed as a function of direction. For each azimuth, dashed lines show the reference speed of 330 m/s. The scale is shown for a single azimuth (at 0°). c)–e) Ray paths in the atmosphere for different directions: c) to the West, d) to the North and e) to the East. Note the different propagation characteristics depending on azimuth.

0.5 km/s (A001A and A002B), and of 0.82 km/s (MODS) (see Figs. 7 and 8).

By coincidence a quarry blast was set off 55 km south-west of the gas hub just four minutes after the gas explosion, potentially generating seismic and acoustic signals that could be misinterpreted as originating from the explosion. Since the origin time and location of the quarry blast were well-known (kindly provided by the Zentralanstalt für Meteorologie und Geodynamik, ZAMG), we calculated expected seismic and acoustic arrival windows for all stations using the same values for propagation velocities as for the explosion signal. The seismic signal of the quarry blast interfered with the arrival time windows of infrasound waves at 4 stations, which were excluded from any further analysis. We inspected also the time windows for infrasound waves from the quarry blast but could not identify any clear acoustic signal on any station. Only at station A010A the time window of a tropospheric-guided infrasound signal from the quarry blast overlaps with the time window of a stratospheric-guided signal from the Baumgarten event, which is why that station was excluded.

4. Acoustic raypath modeling

The observed apparent velocities of the detected signals indicate that the explosion signals are a seismo-acoustic phenomenon and predominantly propagated as infrasound. Hence we model the theoretical propagation of infrasound waves in order to verify our onset picks and to precisely determine the acoustic travel times as well as the highly asymmetric pattern of positive detections. For modeling the infrasound propagation we used the GeoAc raytracing suite that is described in detail by Blom and Waxler (2012) and Blom (2013). We extracted the required atmospheric parameters (wind speed, wind direction, temperature, etc.) from an hourly updated forecast model provided by the European Centre for Medium-Range Weather Forecasts (ECMWF). We compared the forecast-model to data from a weather-balloon measurement that has been conducted on the same day. That comparison is presented and discussed in the online-supplement of this paper. The state of the atmosphere on the day of the explosion changed quickly because of an approaching cold front. For this reason, data from the forecast model at the actual time of the explosion were preferred to radiosonde observations, which are only available at 0 and 12 UTC.

Output from the ECMWF model (cycle 43r3) was retrieved for 08:00 UTC on a latitude–longitude grid with 0.125° resolution. Vertical atmospheric profiles for the 0–78 km altitude range have been produced from the original 137 model levels for the closest grid-point to Baumgarten (Lat, Lon = 48.375, 16.875, in a distance of 6.4 km), which were used to perform 3D raytracing in a stratified atmospheric medium. Since for our network extension of 180 km no thermospheric arrivals are expected, we did not extend the ECMWF model to higher altitudes. From the atmospheric parameters a 3D effective sound speed model is derived, which is highly anisotropic due to the wind direction. Fig. 3a and b show the atmospheric parameters and the effective sound speed model depending on the propagation azimuth. Fig. 3c–e show raytracing results for three different propagation azimuths, representing three characteristic cases. Raytracing towards western directions (Fig. 3c) yields no ray that bends back to the surface within a distance of 200 km. Consequently, from the ray tracing approximation no observation is expected in western directions for this distance range. Raytracing towards northern directions shows a tropospheric waveguide in the lower 5 km that guides the waves to large distances (Fig. 3d). However, no stratospheric phase is expected within 200 km towards North. Towards East tropospheric and stratospheric waveguides are present. Thus towards East both faster and slower phase arrivals are expected. In order to model the spatial bounce-point distribution we performed raytracing from the source allowing for five surface reflections (bounces)

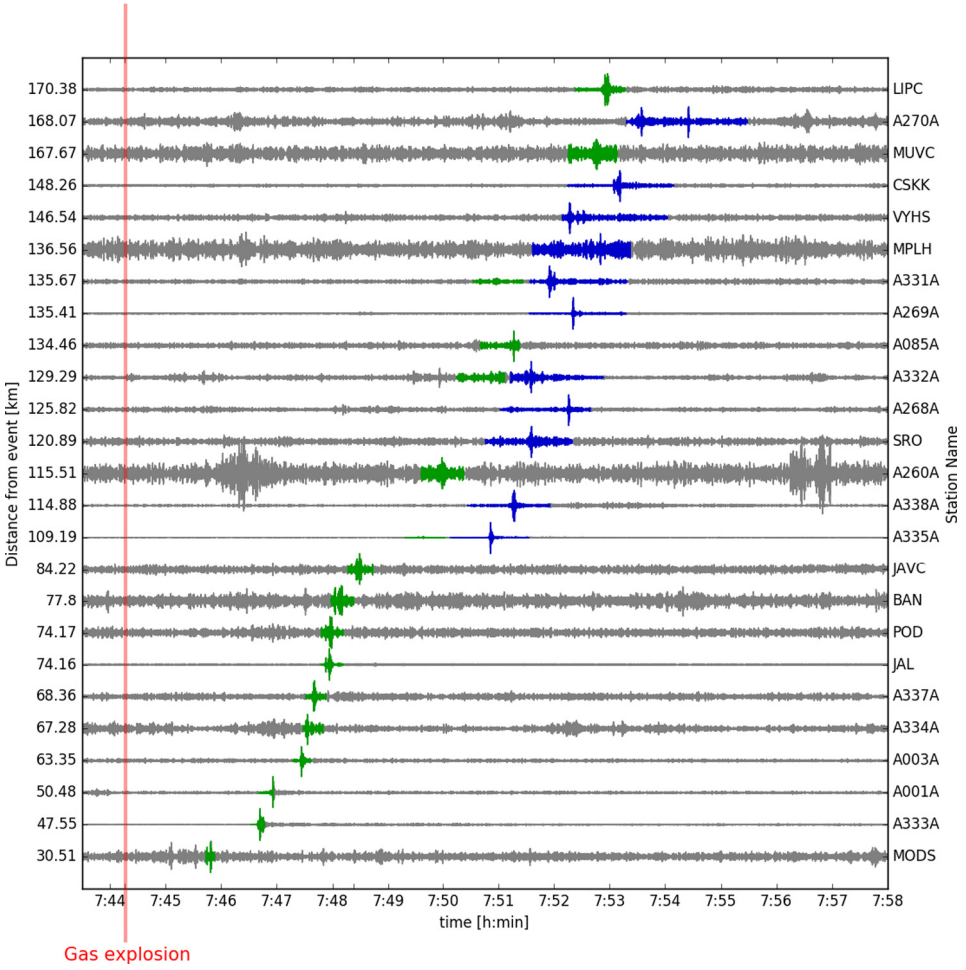

Fig. 4. Selected seismo-acoustic records of the Baumgarten gas explosion (2–4 Hz bandpass-filtered vertical components scaled to individual maximum amplitude). The red line marks the origin time of the gas explosion inferred from ray modeling (see Section 4). Colors highlight the time windows for the arrivals based on the celerity ranges: green for the first (tropospheric-guided) acoustic phase and blue for the second (stratospheric-guided) acoustic phase. The distance increment along the *y*-axis is not constant.

for take-off angles ranging from 0° to 50° (step size 0.5°) and for azimuths ranging from −179° to 180° (step size 1°). GeoAc allows for computation of rays between two specific points, so-called eigenrays. In order to derive the theoretical traveltime of an infrasound signal from Baumgarten to all individual stations where a signal is predicted, we computed all existent eigenrays between Baumgarten and the station locations and attributed them to tropospheric or stratospheric-guided phases. Moreover GeoAc provides amplitudes based on geometrical spreading and frequency-dependent intrinsic attenuation, which is scaled by a tweak parameter. We used the default parameters (frequency = 0.1 Hz and tweak parameter 0.3) for our modeling.

5. Results

5.1. Detections and non-detections of the gas explosion

Due to the highly anisotropic effective sound speeds the propagation of infrasound strongly depends on the azimuth. We modeled the propagation of infrasound from the Baumgarten gas hub by ray tracing, taking into account an appropriate atmospheric model, as described in section 4. Figs. 3c–e show the calculated raypaths and surface bounce distances for various azimuths. The points where the infrasound rays bounce at the surface are plotted on the map in Fig. 5.

Signals from two different celerity ranges have been detected at the stations. The station symbols are color-coded indicating whether a signal from the gas explosion was detected in the faster or the slower celerity range. Green and bluish station symbols indicate phase arrivals from celerities ranging from 318 m/s to 346 m/s and those with celerities ranging from 275 m/s to 310 m/s corresponding to waves guided in the troposphere and stratosphere, respectively. The violet station symbols indicate a detection of both phases. Black station symbols indicate non-detections and for stations labeled with grey colors a seismic signal from the quarry blast event is detected in the time interval of the celerity ranges, which is why those stations are discarded for further processing. The celerity ranges have been deduced with respect to the origin time (7:44:16.2 UTC, determination described in the next section). In principle, the thermosphere could act as third wave guide for acoustic waves, which can be observed on infrasound arrays (see e.g. Ceranna et al., 2009). Yet, due to low particle density and nonlinear dissipation in the upper atmosphere, amplitudes are strongly attenuated within this wave guide (Sutherland and Bass, 2006). Moreover, the lateral offsets of the closest bounce points are usually larger than 300 km, which is more than the aperture of the considered station network. Thus we do not expect to detect any thermospheric phase with our network.

The pattern of detections and non-detections very well matches the bounce-point distribution. There are no surface-bounce points towards western directions (azimuth range 200°–335°). Except

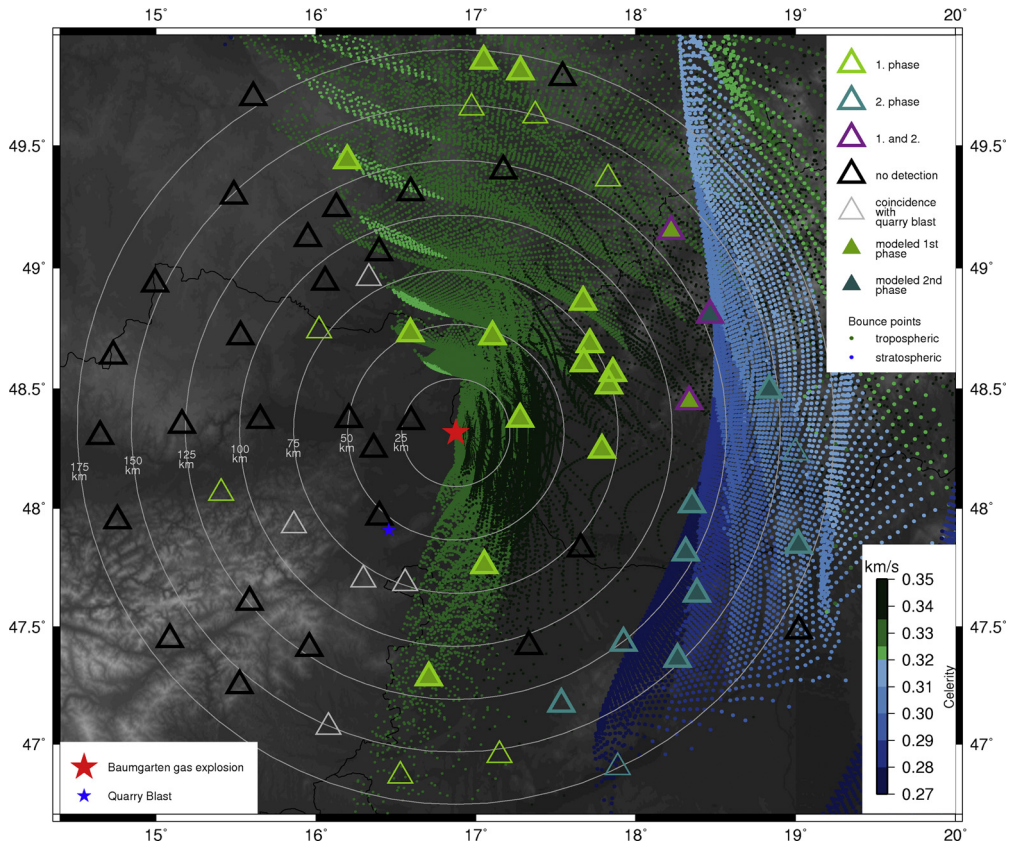

Fig. 5. Map of the seismic stations (triangles) in the wider Vienna region used for this study, and the location of the Baumgarten gas explosion. Station symbols indicate the type of acoustic observations at the stations, to be compared with modeled ray surface bounce points (green/blue dots) and their celerity (distance/travel-time). For station names see Fig. 1.

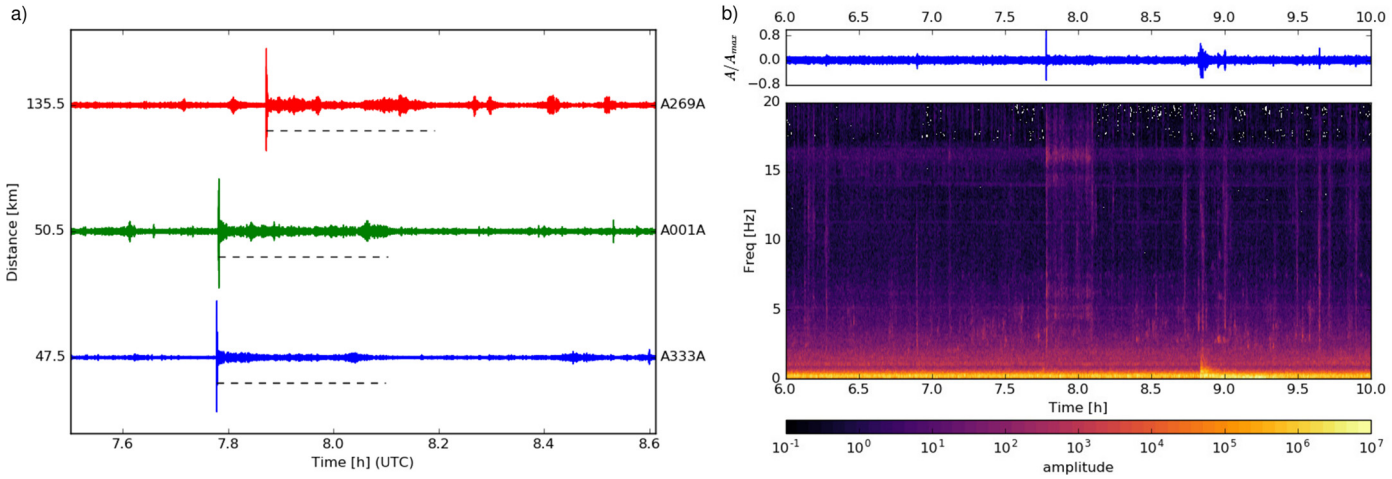

Fig. 6. a) Duration of the continued infrasound signal at the three stations A333A, A001A, and A269A. b) Above: Seismic record, showing normalized amplitudes (A/A_{max}) of the Z-component of station A001A. Below: Spectrogram of station A001A showing the duration and frequency content of the continued signal after the seismo-acoustic arrival of the main blast. At this station the extended coda signal is visible on a broad frequency range (2–20 Hz) between 7.78 h and 8.1 h.

for two stations (A006A and A013A) no station in this azimuth range shows a detection. Towards northern and southern directions (335°–25° and 160°–200°) waves are only guided within the tropospheric waveguide. In northern directions tropospheric phases are observed in large distances (>150 km), which is in agreement with the modeling. Stratospheric guided waves are observed and modeled in eastern directions (25°–160°) in large distances. An observed shadow-zone at stations A337A and A339A in an intermediate distance range and south-eastern directions (120°–180°) is in agreement with the bounce-point distribution from the modeling. The good agreement between observation and modeling confirms the applicability of the atmospheric model and explains the observed pattern. However, some deviations are visible. For stations A331A and A335A we observe two arrivals, where the modeling only predicts a single tropospheric guided wave and the range of stratospheric refractions start at distances 10 to 15 km further to the East. At stations MPLH and A268A south-east of Baumgarten also stratospheric phases are detected although their

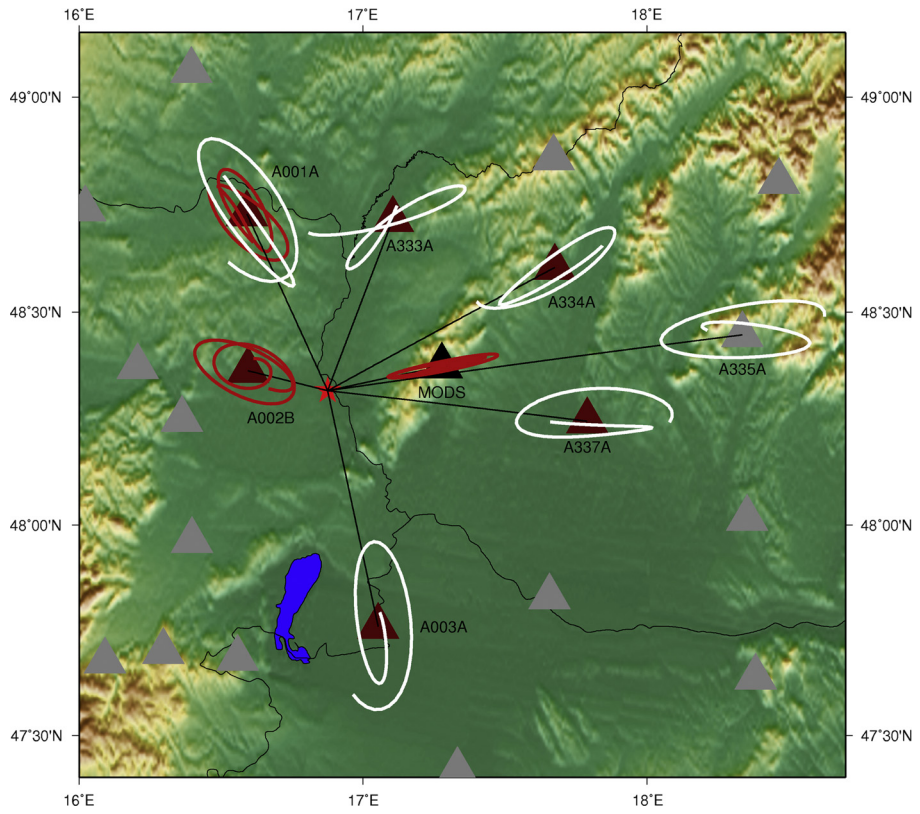

Fig. 7. Particle motion of acoustic (white lines) and seismic (red lines) signals on the horizontal components. Time windows have been selected around the maximum amplitude on the vertical components. Acoustic signals are filtered in the 2–4 Hz and seismic signals in the 0.6–1 Hz frequency bands. Amplitudes are normalized to the maximum amplitude in the horizontal plane.

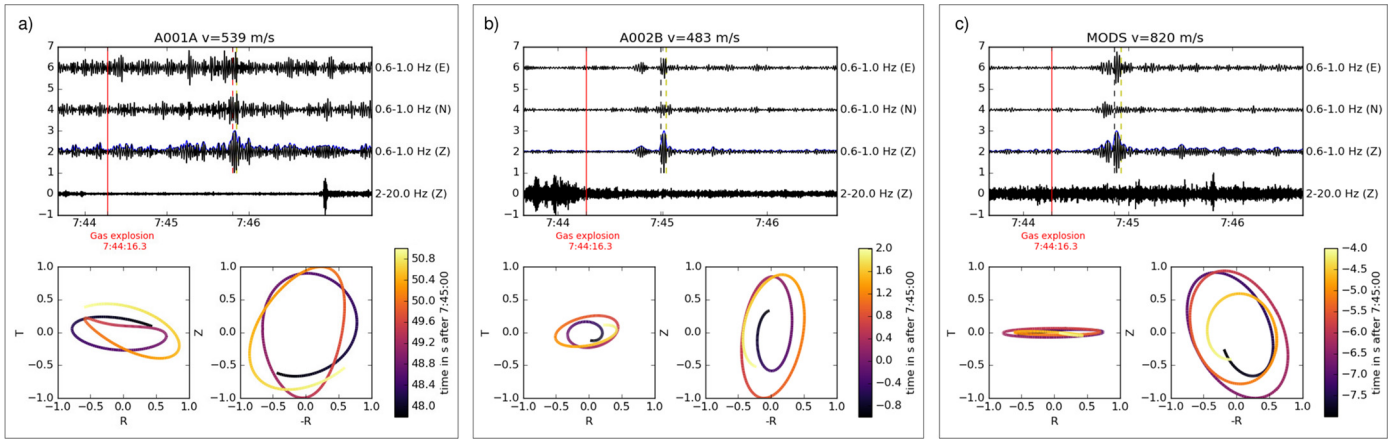

Fig. 8. Seismic signals of the gas explosion on stations A001A (a), A002B (b) and MODS (c). Upper panels: Seismic signal on E, N and Z components filtered in the 0.6–1 Hz, frequency band. At stations A001A and MODS, the Z-component filtered in the 2–20 Hz frequency band shows the later acoustic signal. Dashed lines mark the windows used for the particle motion plot, which have been chosen around the maximum of the envelope of the Z-component (blue-line). The red line indicates the origin time of the gas explosion. Travel-times are derived from the origin time and the maximum of the envelope on the Z-component (blue line). Bottom panels: Particle motion in the R–T (left) and Z–R planes (right). Color represents time (bright = earlier in time, dark = later in time) and indicates a retrograde particle motion.

locations are situated 10 to 15 km West of the modeled area of stratospheric bounce-points. Those stratospheric detections can be explained by deviations of the ECMWF model to the true atmosphere (see Discussion). Potential tropospheric phases that do not match the bounce-point pattern have been detected at two stations west of Baumgarten (A006A and A013A).

5.2. Origin time of the explosion

We determined the origin-time of the gas explosion from the acoustic signal by only using stations that show a clear signal in the data and for which the ray tracing predicts an arrival time of the observed tropospheric or stratospheric phase. Fig. 9 illustrates the source time determination. In total 23 stations have been used, from which 16 stations show clear phases guided within the troposphere and 7 stations show clear phases guided within the stratosphere. In the first column of Table 1 all used stations are listed. In the table the tropospheric and stratospheric detections used for the origin-time estimation are grouped (upper 16 stations and lower 7 stations, respectively). The second column shows the absolute arrival times corresponding to the dashed lines in Fig. 9.

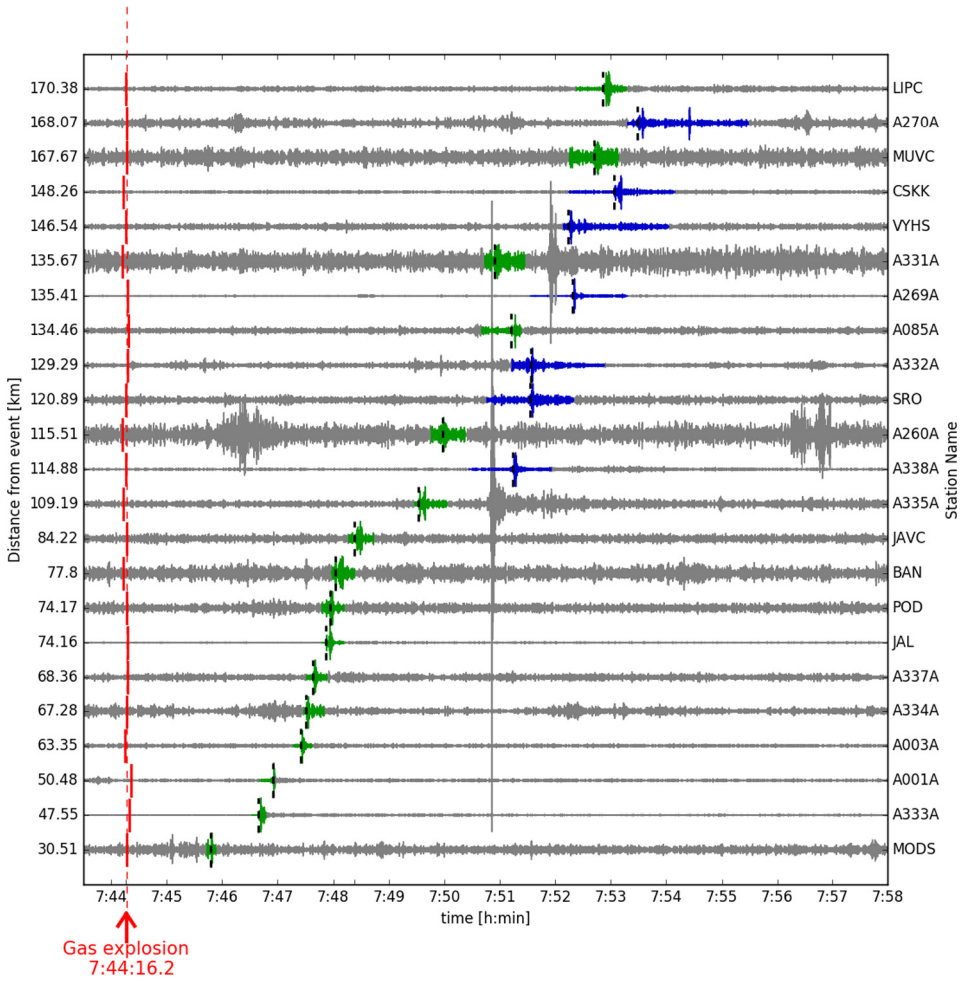

Fig. 9. Illustration of the source-time determination. Seismo-acoustic records from stations reached by modeled rays are shown. Colors highlight the time windows for the arrivals: green for the first (tropospheric-guided) acoustic phase and blue for the second (stratospheric-guided) acoustic phase. The predicted travel-time field is subtracted from observed first arrivals, to yield individual sources time estimates, shown by red lines. The best estimate of source time is given by their average. Predicted arrival times for the tropospheric and stratospheric arrivals are also shown.

For each station, the theoretical travel time has been calculated using the ray tracing procedure described in section 4, which is listed in the third column of Table 1. The estimated origin time, listed in the fourth column for each station is derived by subtracting the theoretical travel time from the observed arrival time. Averaging the estimated origin time over all stations yields the origin time 7:44:16.2 $\pm$ 1 s (UTC). Theoretical and observed celerities are calculated taking into account the mean origin time and the theoretical and observed arrival times, respectively. The resulting celerities for the tropospheric phases range from 318 m/s to 347 m/s, while the celerities from the stratospheric phases range from 274 m/s to 307 m/s, which are in reasonable ranges (Ceranna et al., 2009).

6. Discussion

Identifying the seismo-acoustic wave packet has not been difficult. Yet the details of the waveforms are complex, and not particularly similar from station to station (see supplementary Fig. S3). Amplitudes and signal shape are strongly affected by the atmospheric duct, which is highly anisotropic and allows for multipathing for some directions. As shown in Fig. 3d) and e) multipathing also occurs within the tropospheric wave guide in Eastern directions, which can complicate the detected signal due to multiple phase arrivals. We manually picked only the first onsets of each tropospheric and/or stratospheric signal and considered always the earliest theoretical arrival of the respective phase from the modeling. Moreover, waveforms are complex due to local coupling conditions at the stations. Most seismic stations used in this study were not installed inside a dedicated vault, but rather in basements of more exposed structures such as houses or huts. Fuchs et al. (2015, 2016), Vecsey et al. (2017) and Gráczer et al. (2018) provide a detailed description of seismic vault selection and isolation measures for the majority of the temporary seismic stations used in this study.

Since the seismic sensors are detecting ground motions and not directly air-pressure perturbations, the air-to-ground coupling is an important component to be considered. With acoustic wavelengths of tens to hundreds of meter topographic features may enhance or suppress air-to-ground coupling, resulting in hybrid ray-paths, traveling through air and ground. Nevertheless, the particle motion showed a general radial polarization for the seismo-acoustic arrivals (see Fig. 7). This indicates that the acoustic wave couples into the ground locally at the station, rather than being transmitted to the ground at exposed locations and then being transmitted on pure seismic paths to the stations. In this scenario, it would have been expected that particle motions had pointed towards local coupling spots. Thus, travel times can be derived for the observed phases by purely acoustic modeling.

Signals from gas explosions have been detected by seismometers already before (Koper et al., 2003; Evers et al., 2007). In those studies, the observed apparent velocities of 345–355 m/s on seis-

Table 1
Table of hand-picked absolute observed arrival times, theoretical travel times from raytracing and the resulting origin time. All absolute times are given in UTC.

Station code	Observed arrival	Theoretical travel time (s)	Estimated origin	Deviation from mean (s)	Theoretical celerity (m/s)	Observed celerity (m/s)
MODS	7:45:47.7	91.4	7:44:16.4	0.2	333.9	333.2
A333A	7:46:39.0	139.3	7:44:19.7	3.5	341.3	332.9
A001A	7:46:54.7	153.5	7:44:21.2	5.0	328.8	318.3
A003A	7:47:24.8	189.7	7:44:15.1	−1.04	334.0	335.8
A334A	7:47:30.3	193.6	7:44:16.7	0.5	347.5	346.5
A337A	7:47:37.5	199.9	7:44:17.5	1.4	341.9	339.6
JAL	7:47:52.0	214.1	7:44:17.9	1.7	346.4	343.6
POD	7:47:56.9	219.8	7:44:17.2	1.0	337.5	335.9
BAN	7:48:02.3	228.8	7:44:13.5	−2.7	340.0	344.0
JAVC	7:48:23.3	246.8	7:44:16.5	0.34	341.3	340.8
A335A	7:49:32.4	319.7	7:44:12.7	−3.5	341.5	345.3
A260A	7:49:58.3	346.6	7:44:11.7	−4.5	333.2	337.6
A331A	7:50:54.4	402.3	7:44:12.1	−4.0	337.2	340.7
A085A	7:51:11.8	413.3	7:44:18.5	2.3	325.3	323.5
MUVC	7:52:42.3	505.6	7:44:16.7	0.5	331.6	331.3
LIPC	7:52:51.4	515.4	7:44:16.0	−0.2	330.6	330.7
A338A	7:51:13.8	418.1	7:44:15.7	−0.5	274.8	275.1
A332A	7:51:33.4	436.1	7:44:17.3	1.11	296.4	295.7
SRO	7:51:32.9	437.3	7:44:15.6	−0.6	276.4	276.8
VYHS	7:52:13.7	477.6	7:44:16.1	−0.08	306.8	306.9
A269A	7:52:18.7	480.8	7:44:17.9	1.8	281.7	280.6
CSKK	7:53:03.4	530.1	7:44:13.3	−2.9	279.7	281.2
A270A	7:53:28.4	551.7	7:44:16.7	0.5	304.6	304.4
Standard deviation:				2.3 s		
Error of mean:				0.5 s		
Mean origin time:			07:44:16.15 ± 0.5 s			

mometers in distances of less than 80 km have been interpreted as being the expression of air-coupled Rayleigh waves. In contrast, in our study, successful modeling of the spatial detection/non-detection-pattern proves at least for the Baumgarten incident that acoustic waves in the atmosphere are responsible for the propagation of energy between the source and seismic receivers.

The agreement between the observed and predicted spatial patterns of observations is quite striking, especially since little local meteorological information has been used. The balloon data and the ECMWF model differ in the level of detail they provide (see Supplementary Section). Smoothed forecast models (as used in this study) may underpredict the intensity of tropospheric waves since contrasts in reality might be sharper, as evidenced by the balloon data. However, this did not cause any larger observation-to-model discrepancies for this study. It might still explain some of the positive detections of the slower acoustic phase that have been observed at stations located a few kilometers west of the modeled bounce-point distribution for stratospheric guided waves: Even if the atmospheric models from ECMWF have been found to be broadly consistent with wind radiosonde measurements up to altitudes of 40 km (Le Pichon et al., 2015), the specific local weather conditions at Baumgarten at the day of the explosion yield for altitudes exceeding 24 km larger deviations from the ECMWF data (see supplementary Fig. S4). Thus raypaths of stratospheric phases are possibly affected by those deviations. Measured data are only available up to 32 km altitude. The modeled turning heights for the closest bounce-points of stratospheric phases are in the 35–40 km range, where the two models can not be compared directly. However, high zonal winds at 30–32 km cause the stratospheric inversion of the effective sound speed to be at shallower altitudes for the measured data. If this tendency continued to higher altitudes the shallower inversion would turn the rays back to the surface at closer locations to Baumgarten than those modeled from the ECMWF model, which would explain the detections of stratospheric phases at closer locations. Additionally, deviations of the real effective sound speed can be imprinted by gravity waves which can change the atmospheric duct dynamically (Pilger et al., 2013; Hedlin and Drob, 2014), which is not taken into account in this study.

This study may have been fortuitous in that a cold front has passed just before the accident, creating meteorological conditions that are particularly favorable for recording acoustic waves over a large range of distances. Still, even under less favorable conditions, the high data density provided by the AlpArray network makes it appear very likely that the event would have been recorded in any case, although perhaps only via stratospheric arrivals.

The observations have provided useful information on the Baumgarten accident, namely the origin time, and the potential duration of the burning. The origin time of 7:44:16.2 ± 1 s (UTC) was determined by taking into account the observations at 23 receivers. The uncertainty is derived by the scatter of the origin times at the individual stations (see Fig. 9 and supplementary Fig. S3). A standard deviation of 2.3 s yields a standard error (error of the mean) of 0.5 s (see Table 1). However, this uncertainty does not take into account any systematic errors due to deviations of the atmospheric model.

The extended coda signal is observed only on three stations with high signal-to-noise ratio. A clear cut-off of this signal is only observed at one station (A001A), where the signal is recorded in a broad frequency range (1–20 Hz) for 19 min. This is in agreement with eyewitness reports testifying a duration of the fire of 15–20 min. Continuous acoustic signals created by large fires have been observed on infrasound stations before (Arrowsmith et al., 2012), confirming the potential of large fires to be observed acoustically. Koper et al. (2003) reported on the observation of gas-flow and fire, which both apparently generated acoustic signals. Their distinct onset times allowed them to be separated and after the first sharp pulses the fire also created a strong and lasting infrasound signal. At the Baumgarten incident we are not able to resolve two separate events, which may indicate that the ignition

of the gas happened essentially at the same time as the release of the gas.

The seismic signal that we have observed is most prominent in the 0.6–1 Hz frequency band. It shows radial polarization and retrograde particle motion (see Figs. 7 and 8). Thus it is most likely a regional Rayleigh wave phase (Rg) which is guided in the uppermost layer of the crust. We observe a large scatter of very small group velocities of around 500 to 800 m/s. Rg-phases are known to have large regional variations (Koper et al., 2003). In sedimentary basins, short-period crustal Rayleigh waves can have quite slow group velocities. Chung and Yeh (1997) observed group velocities from earthquakes filtered in the same frequency range (0.6–1 Hz) ranging from 650 to 900 m/s in distance ranges from 20–50 km, which is comparable to the distance and velocity ranges that we observe and which is explained by the presence of a shallow alluvial sedimentary layer. However, since we do not have access to a shallow velocity model for the region around Baumgarten, we so far can not use the observed seismic signal to reveal any more information about the event.

7. Conclusion

We have presented seismo-acoustic observations from the Baumgarten accident in Austria. The strong acoustic waves that have been generated by the explosion have been observed to distances of up to more than 150 km, mainly on seismic stations of the AlpArray. Modeling of the infrasound wave propagation has allowed to interpret the observations: the waves have propagated along acoustic ducts in the troposphere and the stratosphere. The good fit between observed and modeled patterns of infrasound detections has allowed to determine a precise (within one second) and independent origin time of the accident, as well as the duration of the protracted period of gas release and fire. Clearly, seismological recordings of infrasound can be rather useful for forensic investigations. Moreover, it is demonstrated that dense seismic networks as the AlpArray can map the infrasound field with high spatial resolution. As described by Chunchuzov et al. (2014) and Hedlin and Drob (2014) this could be further utilized, e.g., to infer unresolved dynamical properties of the atmosphere and thus for improving meteorological models by seismological observations.

8. Data availability

This study is based on seismic waveform data from the temporary AlpArray network (code Z3) and several permanent and temporary local seismic networks in central Europe (codes OE, CZ, HU, SK, M1 and D1). By decision of the AlpArray network operators data from the Z3 network is not publicly available at the time of publication. Please see the project homepage for details on data access: www.alparray.ethz.ch (last accessed March 2018). Waveform data from the permanent seismic networks with codes OE, CZ, HU, SK and M1 is freely available at the European Integrated Data Archive (EIDA): www.orfeus-eu.org/data/eida (last accessed March 2018). Data from the small-scale network D1 is available upon request (doi:10.7914/SN/D1). Stations JAL, POD and BAN are part of the CzechGeo-MKnet and data are available upon request at www.irsm.cas.cz/index_en.php?page=mknet_en (last accessed March 2018).

Data from the weather balloon is freely available at the University of Wyoming: http://weather.uwyo.edu/upperair/sounding.html (last accessed March 2018). The atmospheric model used for this study is the December 12, 2018, 08:00 UTC forecast model of the European Center for Medium Range Weatherforecast. The model is available at (www.ecmwf.int, last accessed March 2018).

Acknowledgements

We acknowledge the operation of the AlpArray temporary seismic network (Hetényi et al., 2018) and the permanent seismic networks used in this study: CZ net (Institute of Geophysics, Academy of Sciences of the Czech Republic, 1973), HU net (Kovesligethy Rado Seismological Observatory (Geodetic and Geophysical Institute, Research Centre for Astronomy and Earth Sciences, Hungarian Academy of Sciences (MTA CSFK GGI KRSZO)), 1988), IPE EDU net (D1) (Institute of Physics of the Earth Masaryk University Brno, 2014), MONET (M1) (Institute of Physics of The Earth Masaryk University Brno (IPE), 2017), OE net (www.zamg.ac.at, last accessed March 2018) and SK net (ESI SAS (Earth Science Institute of The Slovak Academy of Sciences), 2004). Additionally we thank the operators of the CzechGeo-MKnet network in Little Carpathian seismic zone for sharing the seismic data. The CzechGeo-MKnet network is operated in cooperation with the Institute of Rock Structure and Mechanics, Academy of Sciences of the Czech Republic, the Earth Science Institute of The Slovak Academy of Sciences and the company ProgSeis s.r.o.

The Python Toolbox ObsPy (Beyreuther et al., 2010) was used for various processing and data handling purposes and GMT (Wessel and Smith, 1991) for production of maps. To model the propagation of infrasound the GeoAc raytracer was used (developed by Philip Blom), which is kindly provided on GitHub (https://github.com/LANL-Seismoacoustics/GeoAc, last accessed March 2018). We acknowledge financial support by the Austrian Science Fund (FWF) projects P 26391 and P 30707, and the Vienna Science and Technology Fund (WWTF) project MA14-006. We thank Ulrike Mitterbauer and Rita Meurers from Zentralanstalt für Meteorologie und Geodynamik (ZAMG) for providing information on the quarry blast, as well as Christoph Pilger and Lars Ceranna from the German Federal Institute for Geosciences and Natural Resources (BGR) for fruitful discussions.

AlpArray was made possible by the AlpArray Seismic Network Team:

György HETÉNYI, Rafael ABREU, Ivo ALLEGRETTI, Maria-Theresia APOLONER, Coralie AUBERT, Simon BESANÇON, Maxime BÉS DE BERC, Götz BOKELMANN, Didier BRUNEL, Marco CAPELLO, Martina ČARMAN, Adriano CAVALIERE, Jérôme CHÉZE, Claudio CHIARABBA, John CLINTON, Glenn COUGOULAT, Wayne C. CRAWFORD, Luigia CRISTIANO, Tibor CZIFRA, Ezio D'ALEMA, Stefania DANESI, Romuald DANIEL, Anke DANNOWSKI, Iva DASOVIĆ, Anne DESCHAMPS, Jean-Xavier DESSA, Cécile DOUBRE, Sven EGDORF, ETHZ-SED Electronics Lab, Tomislav FIKET, Kasper FISCHER, Wolfgang FRIEDERICH, Florian FUCHS, Sigward FUNKE, Domenico GIARDINI, Aladino GOVONI, Zoltán GRÁCZER, Gidera GRÖSCHL, Stefan HEIMERS, Ben HEIT, Davorka HERAK, Marijan HERAK, Johann HUBER, Dejan JARIĆ, Petr JEDLIČKA, Yan JIA, Hélène JUND, Edi KISSLING, Stefan KLINGEN, Bernhard KLOTZ, Petr KOLÍNSKÝ, Heidrun KOPP, Michael KORN, Josef KOTEK, Lothar KÜHNE, Krešo KUK, Dietrich LANGE, Jürgen LOOS, Sara LOVATI, Deny MALENGROS, Lucia MARGHERITI, Christophe MARON, Xavier MARTIN, Marco MASSA, Francesco MAZZARINI, Thomas MEIER, Laurent MÉTRAL, Irene MOLINARI, Milena MORETTI, Helena MUNZAROVÁ, Anna NARDI, Jurij PAHOR, Anne PAUL, Catherine PÉQUEGNAT, Daniel PETERSEN, Damiano PESARESI, Davide PICCININI, Claudia PIROMALLO, Thomas PLENEFISCH, Jaroslava PLOMEROVÁ, Silvia PONDRELLI, Snježan PREVOLNIK, Roman RACINE, Marc RÉGNIER, Miriam REISS, Joachim RITTER, Georg RÜMPKER, Simone SALIMBENI, Marco SANTULIN, Werner SCHERER, Sven SCHIPPKUS, Detlef SCHULTE-KORTNACK, Vesna ŠIPKA, Stefano SOLARINO, Daniele SPALLAROSSA, Kathrin SPIEKER, Josip STIPČEVIĆ, Angelo STROLLO, Bálint SÜLE, Gyöngyvér SZANYI, Eszter SZŰCS, Christine THOMAS, Martin THORWART, Frederik TILMANN, Stefan UEDING, Massimiliano VALLOCCHIA, Luděk VECSEY, René VOIGT, Joachim WASSERMANN, Zoltán WÉBER, Chris-

tian WEIDLE, Viktor WESZTERGOM, Gauthier WEYLAND, Stefan WIEMER, Felix WOLF, David WOLYNIEC, Thomas ZIEKE, Mladen ŽIVČIĆ.

Appendix A. Supplementary material

Supplementary material related to this article can be found online at https://doi.org/10.1016/j.epsl.2018.08.034.

References

Aleqabi, G.I., Wysession, M.E., Ghalib, H.A.A., 2015. Characterization of seismic sources from military operations in Urban Terrain (MOUT): examples from Baghdad. Bull. Seismol. Soc. Am. 106, 23–41.

Arrowsmith, S., Whitaker, R., Le Pichon, A., Cansi, Y., Brachet, N., Charbit, M., Park, J., Stump, B., Che, I.-Y., 2012. Development and validation of infrasound data processing algorithms. In: Proceeding of the 2012 Monitoring Research Review: Ground-Based Nuclear Explosion Monitoring Technologies 2, pp. 665–675.

Beyreuther, M., Barsch, R., Krischer, L., Megies, T., Behr, Y., Wassermann, J., 2010. ObsPy: a Python toolbox for seismology. Seismol. Res. Lett. 81 (3), 530.

Blom, P., 2013. Interaction of the Cyclonic Winds with the Infrasonic Signal Generated by a Large Maritime Storm. Dissertation, University of Mississippi. ProQuest/UMI (UMI No. 3567512).

Blom, P., Waxler, R., 2012. Impulse propagation in the nocturnal boundary layer: analysis of the geometric component. J. Acoust. Soc. Am. 131 (5), 3680–3690.

Ceranna, L., Le Pichon, A., Green, D.N., Mialle, P., 2009. The Buncefield explosion: a benchmark for infrasound analysis across Central Europe. Geophys. J. Int. 177, 491–508.

Chunchuzov, I., Kulichkov, S., Popov, O., Hedlin, M., 2014. Modeling propagation of infrasound signals observed by a dense seismic network. J. Acoust. Soc. Am. 135 (1), 38–48.

Chung, J.-K., Yeh, Y.T., 1997. Shallow crustal structure from short-period Rayleigh-wave dispersion data in southwestern Taiwan. Bull. Seismol. Soc. Am. 87 (2), 370–382.

ESI SAS (Earth Science Institute of The Slovak Academy of Sciences), 2004. National Network of Seismic Stations of Slovakia. Deutsches GeoForschungsZentrum GFZ.

Evers, L.G., Ceranna, L., Haak, H.W., le Pichon, A., Whitaker, R.W., 2007. A seismoacoustic analysis of the gas-pipeline explosion near Ghislenghien in Belgium. Bull. Seismol. Soc. Am. 97, 417–425.

Fuchs, F., Kolínský, P., Gröschl, G., Apoloner, M.-T., Qorbani, E., Schneider, F., Bokelmann, G., 2015. Site selection for a countrywide temporary network in Austria: noise analysis and preliminary performance. Adv. Geosci. 41, 25–33.

Fuchs, F., Kolínský, P., Gröschl, G., Bokelmann, G., The AlpArray Working Group, 2016. AlpArray in Austria and Slovakia: technical realization, site description and noise characterization. Adv. Geosci. 43, 1–13.

Gráczer, Z., Szanyi, G., Bondár, I., Czanik, C., Czifra, T., Győri, E., Hetényi, G., Kovács, I., Molinari, I., Süle, B., Szűcs, E., Wesztergom, V., Wéber, Z., the AlpArray Working Group, 2018. AlpArray in Hungary: temporary and permanent seismological networks in the transition zone between the Eastern Alps and the Pannonian basin. Acta Geod. Geophys.

Green, D.N., Vergoz, J., Gibson, R., le Pichon, A., Ceranna, L., 2011. Infrasound radiated by the Gerdec and Chelopechene explosions: propagation along unexpected paths. Geophys. J. Int. 185, 890–910.

Hedlin, M., Drob, D.P., 2014. Statistical characterization of atmospheric gravity waves by seismoacoustic observations. J. Geophys. Res., Atmos. 119 (9), 5345–5363.

Hetényi, G., Molinari, I., Clinton, J., Bokelmann, G., Bondár, I., Crawford, W.C., Dessa, J.-X., Doubre, C., Friederich, W., Fuchs, F., Giardini, D., Gráczer, Z., Handy, M.R., Herak, M., Jia, Y., Kissling, E., Kopp, H., Korn, M., Margheriti, L., Meier, T., Mucciarelli, M., Paul, A., Pesaresi, D., Piromallo, C., Plenefisch, T., Plomerová, J., Ritter, J., Rümpker, G., Sipka, V., Spallarossa, D., Thomas, C., Tilmann, F., Wassermann, J., Weber, M., Wéber, Z., Wesztergom, V., Zivcic, M., the AlpArray Seismic Network Team, the AlpArray OBS Cruise Crew, the AlpArray Working Group, 2018. The AlpArray seismic network: a large-scale European experiment to image the Alpine orogen. Surv. Geophys. 39 (5), 1009–1033.

Hinzen, K.-G., 2014. Seismic analysis of the Accidental WWII bomb explosion in Euskirchen, Germany, on 3 January 2014. Seismol. Res. Lett. 85, 825–835.

Hong, T.-K., 2011. Seismic investigation of the 26 March 2010 sinking of the South Korean Naval Vessel Cheonanham. Bull. Seismol. Soc. Am. 101, 1554–1562.

Institute of Geophysics, Academy of Sciences of the Czech Republic, 1973. Czech Regional Seismic Network, International Federation of Digital Seismograph Networks.

Institute of Physics of the Earth Masaryk University Brno, 2014. IPE EDU, International Federation of Digital Seismograph Networks, Other/Seismic Network.

Institute of Physics of the Earth Masaryk University Brno (IPE), 2017. MOravia NETwork (MONET). GFZ Data Services.

Koper, K.D., Wallace, T.C., 2001. Forensic seismology and the sinking of the Kursk. Eos 82, 37–52.

Koper, K.D., Wallace, T.C., Aster, R.C., 2003. Seismic recordings of the Carlsbad, New Mexico, pipeline explosion of 19 August 2000. Bull. Seismol. Soc. Am. 93, 1427–1432.

Koper, K.D., Wallace, T.C., Hollnack, D., 1999. Seismic Analysis of the 7 August 1998 truck-bomb blast at the American Embassy in Nairobi, Kenya. Seismol. Res. Lett. 70, 512–521.

Koper, K.D., Wallace, T.C., Reinke, R.E., Leverette, J.A., 2002. Empirical scaling laws for truck bomb explosions based on seismic and acoustic data. Bull. Seismol. Soc. Am. 92, 527–542.

Kovesligethy Rado Seismological Observatory (Geodetic and Geophysical Institute, Research Centre for Astronomy and Earth Sciences, Hungarian Academy of Sciences (MTA CSFK GGI KRSZO)), 1988. Hungarian National Seismological Network. Deutsches GeoForschungsZentrum GFZ.

Kristekova, M., Moczo, P., Labak, P., Cipciar, A., Fojtikova, L., Madaras, J., Kristek, J., 2008. Time–frequency analysis of explosions in the ammunition factory in Novaky, Slovakia. Bull. Seismol. Soc. Am. 98, 2507–2516.

Le Pichon, A., Assink, J.D., Heinrich, P., Blanc, E., Charlton-Perez, A., Lee, C.F., Keckhut, P., Hauchecorne, A., Rüfenacht, R., Kämpfer, N., Drob, D.P., Smets, P.S.M., Evers, L.G., Ceranna, L., Pilger, C., Ross, O., Claud, C., 2015. Comparison of co-located independent ground-based middle atmospheric wind and temperature measurements with numerical weather prediction models. J. Geophys. Res., Atmos. 120 (16), 8318–8331.

Nippress, A., Green, D.N., Marcillo, O.E., Arrowsmith, S.J., 2014. Generating regional infrasound celerity-range models using ground-truth information and the implications for event location. Geophys. J. Int. 197, 1154–1165.

Ottemöller, L., Evers, L.G., 2008. Seismo-acoustic analysis of the Buncefield oil depot explosion in the UK, 2005 December 11. Geophys. J. Int. 182, 1123–1134.

Pilger, C., Streicher, F., Ceranna, L., Koch, K., 2013. Application of propagation modeling to verify and discriminate ground-truth infrasound signals at regional distances. InfraMatics 2, 39–55.

Sutherland, L.C., Bass, H.E., 2006. Atmospheric absorption in the atmosphere up to 160 km. J. Acoust. Soc. Am. 120 (5), 2985.

Vecsey, L., Plomerova, J., Jedlicka, P., Munzarova, H., Babuska, V., The AlpArray Working Group, 2017. Data quality control and tools in passive seismic experiments exemplified on the Czech broadband seismic pool MOBNET in the AlpArray collaborative project. Geosci. Instrum. Method. Data Syst. 6, 505–521.

Walker, K.T., Shelby, R., Hedlin, M.A., de Groot-Hedlin, C., Vernon, F., 2011. Western U.S. infrasonic catalog: illuminating infrasonic hot spots with the usarray. J. Geophys. Res. 116, B12305.

Wessel, Paul, Smith, Walter H.F., 1991. Free software helps map and display data. Eos, Trans. Am. Geophys. Union 72 (41), 441–446.